

Microstructures and Crystal Size Distribution (CSD) of Chromites from Gysian Silvana Ophiolite Serpentinites, Urmia, Iran

M. Modjarrad*

Faculty of Sciences, Department of Geology, Urmia University, Urmia, Islamic Republic of Iran

Received: 17 July 2022 / Revised: 11 June 2023 / Accepted: 22 June 2023

Abstract

One of the components of Gysian Silvana ophiolite in the south of Urmia and the continuation of the Neo-Tethys in the northwestern of Iran is serpentinites with lizardite/chrysotile and magnetite phases as the main mineral and chromite (Cr-spinel) and some rare olivine and orthopyroxenes. A variety of microstructures such as mesh, sieve, lamellar, fibrous, and hourglass were identified. The existence of lizardite plates (001) crosswise in the margin of a low crystallized mass nucleus of net texture is determined by microstructures. Due to the lack of antigorite in the serpentinites, the depth of subduction of the Neo-Tethys slab in this part of Iran may be low. The crystal size distribution (CSD) of the Gysian serpentinite chromites was studied. We discriminate three types of CSD patterns for chromite crystals, extract nucleation, and growth parameters from intercept and slope values of the patterns. The first type is a linear steady-state pattern with a nucleation rate/growth rate (J/G) of about 12 and $Gt=1.28$; the second type has a non-linear concave downtrend which is the result of annealing or Ostwald ripening at a small size part with $J/G=13-15$ and $Gt=1.33$. The third type is complex and shows nucleation density with two separate parts. It could be modeled by two crystal populations, small and large sizes overlapping linear patterns. The J/G for small crystals was twice for large sizes and multiple nuclei have less growth. The Gt was 1.60 for small and 1.10 for those large sizes. Assuming the constant crystal growth rate in silicate materials is 10^{-9} cm/s, the time for the growth of large chromites is six times longer than that of small crystals. These two segmental CSD patterns probably present arising processes or alteration production of mafic minerals as small chromites.

Keywords: Chromite; CSD; Gysian; Urmia; Iran.

Introduction

According to the manner and style of placement, ophiolites are divided into the following two categories (1, 2): active marginal ophiolites, in which ophiolite spots

are found in ruptures inside, and active continental margins, and often they have a melange form and, secondly, the ophiolites of the collision zones are found at the collision of the plates. Serpentinization is one of the most common alteration processes in ophiolites

* Corresponding author: Tel: +98 9143450452; Email: m.modjarrad@urmia.ac.ir

through which chemical reactions of water with peridotites produce serpentine group minerals including chrysotile, lizardite, and antigorite (3, 4). According to some researchers, studying how serpentinites is formed could have critical applications for understanding the large-scale geodynamics of that area (5, 6). Serpentinization occurs in a vast range of pressures and temperatures. A principal story of subduction zones is the return (recirculation) of hydrated rocks into the mantle and the so-called "subduction factory" (7). The progression of serpentinization causes a decrease in the seismic velocity of rocks (8).

The texture of rocks and parameters such as size offers important evidence about the petro-physical procedures complicated in rock formation (9-12). The CSD analysis eventually improves our knowledge of magmatic progressions. Therefore, the crystal size analysis should be added to other experimental and

geochemical studies to obtain more complete results from the origin of the magma. One of the key features of numerical textural studies is the dispersal of crystal sizes. However, the study on the matter was started 120 years ago, but until 30 years ago, the investigations did not obtain much development. The main paper by Cashman and Marsh (13) focused on this subject.

Geological setting

Gysian region is located in the geological map of 1: 10,000 Silvana (14) in the south of Urmia between longitudes of N44' 44" to 44' 56" and latitudes of E37' 07" to 37' 16". This region is a continuation of the northwest of the Sanandaj-Sirjan zone in terms of structural location. Sanandaj-Sirjan zone, the most complex structural zone in Iran, and the Palaeozoic and Mesozoic rocks have been marked by at least two syn-

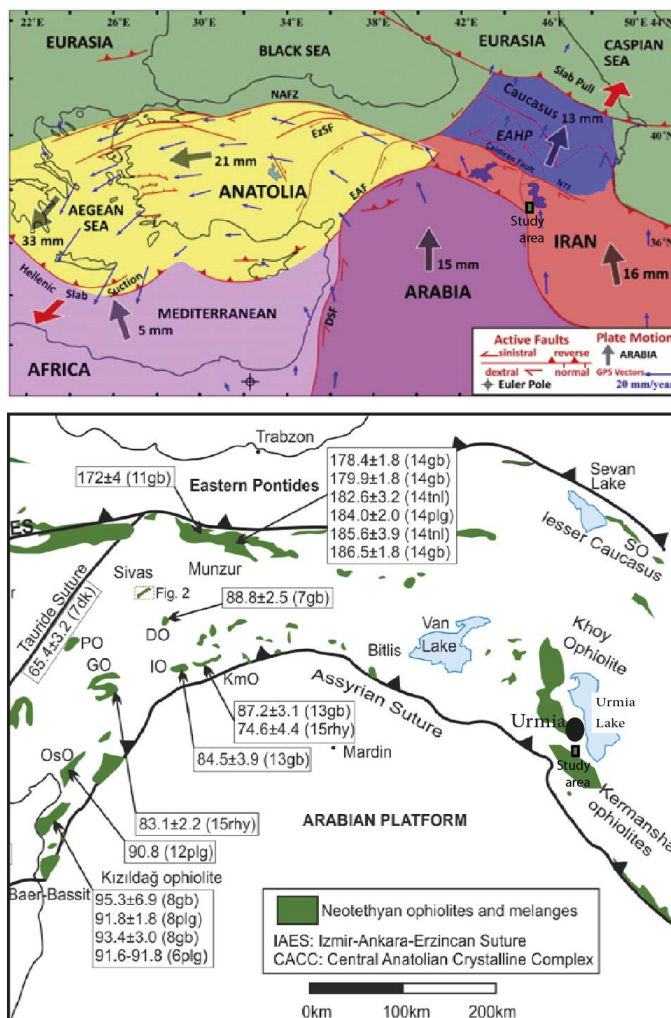


Figure 1. Location of Northwest of Iran (study area) in large scale geodynamic map of the region in relation to the Neo-Tethys subduction between the Arabian plate and Central Iran micro-continents.

tectonic dynamo-thermal deformations (15). This zone is part of the Zagros Mountains and the Alpine-Himalayan Orogenic System, which is formed by the convergence between the northern part of Gondwana and southern Eurasia (16). The direct direction of this zone in the distance between Urmia and Esfandageh locally represents the strike-slip system, which shows the dominance of the shear tectonic regime (straight line) at the junction of two Arabian-Iranian tectonic plates (17-18). The Sanandaj-Sirjan area extends from the Sabzevaran fault in the southeast to the Turkish-Iranian border in northwestern Iraq and from there to southeastern Anatolia, Turkey (Figure 1). Neo-Thetys

subduction probably began in the Cretaceous (19). Subduction to the north of Neo-Tethys in the Early Jurassic (below the Turan platform in Eurasia) separates a new set of northwestern trends from the passive margin of Gondwana, including the Sanandaj-Sirjan subcontinent and the Lesser Caucasus (20) and the subcontinents of Kirsehir and Sakarya in Turkey (21) and the formation of the Pindos Ocean (20).

Security considerations have so far prevented detailed studies in the Iran-Iraq boundary, so this article is one of the first introduces of the Gysian Silvana ophiolite in southern Urmia (Figure 2a). So far, there has been no ophiolite spot in large-scale maps of the foothills of

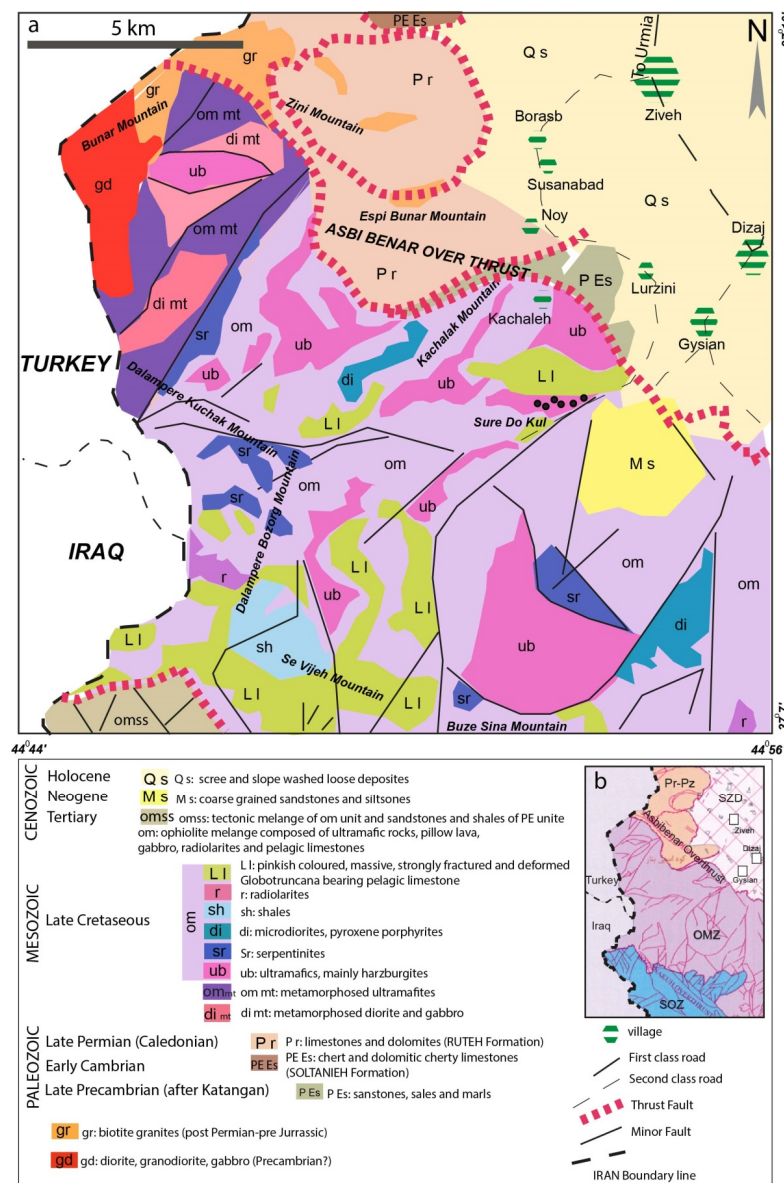


Figure 2. a: Simplified geological map of the Gysian Silvana ophiolitic region (14). b: The Silvana ophiolite subzones.

southeastern Turkey in Hakkari province (eastern Turkey), including the Goleman and Elazig ophiolites (22); after entering Iran, the ophiolites of Kermanshah (23) and Kurdistan Province. The author hopes to present the results of this research as a starting point for research on these ophiolites. The age of the ophiolite formation is most likely the Late Upper Cretaceous to Paleocene, such as another part of the Sanandaj-Sirjan zone, related to the NeoTethys ocean subduction. Ar-Ar, dating from the ophiolite rocks of Dalamper Mountain, Silvana, shows an age of 94 Ma (24).

Structurally, the Silvana region is divided into five sub-zones (Figure 2b): The ophiolite mixed zone (OMZ), which is characterized by a reverse thrust fault from the north with the Silvana-Ziveh depression zones (SZD), Precambrian-Paleozoic unit (Pr-Pz) and Molasses unit (Mo) is bordered and adjacent to the south with the ophiolite-sedimentary mixed zone (SOZ) and metamorphic zone (MZ).

Materials and Methods

For petrophysical parameters measurement, we practice 2D thin section microphotographs of the samples, using whole slide imaging, microvisioner technique, classified the images, and analyze the file using image processing software, Digimizer for measuring width, length, area, and crystals roundness. CSDCorrections software (25) was used to calculate the CSD patterns in 3D, slope, and intercept values of the curve.

Results

Microstructures

Orthopyroxene crystals are usually altered around or along with fractures and become bastites or other secondary minerals. Basting begins in the presence of existing fractures and gradually takes over the entire crystal. Excess iron is dispersed in the form of magnetite around the crystal, making it easier to identify the mineral boundaries (magnesium-containing components have migrated to serpentine). This is normal in serpentinites (26). Lizardites are low-temperature serpentine minerals that form at lower temperatures (260°C) and are among the most common minerals formed in olivine pseudomorphs. They were significantly found in the lower degrees of metamorphism of the greenschist facies, and due to progressive metamorphism up to the top of the greenschist facies, they converted into high-temperature serpentine polymorphs (27).

In the microscopic sections of the study area, the serpentinization of the olivines began around the crystal and its fractures and expanded to lizardite. Due to

progressive serpentinization, no trace of pseudomorphic olivine remains, and only serpentine mineral is seen along with magnetite. The mineral content of lizardite was high. Chrysotile begins to grow in the rock when there are olivines left in the rock, and they have become lizardite sheets. At this stage, the chrysotile begins to grow as very thin fibrous in the veins. Chrysotile fibers need support for nucleation and growth, and when used to grow from the wall surface, they use the exact location as support. This type of nucleation is called heterogeneous nucleation. Chrysotile is detectable in fibrous form and is more common in fractures and fissures in the form. It grows in the form of thin blades utterly perpendicular to the fracture wall. In general, two types of chrysotile filaments are seen in the study area vertical chrysotile filaments, and the other is oblique filaments. The presence of chrysotiles in the form of cross fibers in the background of other serpentine minerals indicates the delayed formation of chrysotiles under static conditions. In addition to chromite (cr-spinel crystals), which are coarse-grained and brown in plane-polarized light with a skeletal texture, they are sometimes found in sections of opaque minerals (magnetite). These minerals are finely dispersed throughout the section. Mesh texture is prevalent in these rocks. The serpentine from these textures is lizardite. The streaks around the olivine follow precisely the original shape of the crystal. If the primary fractures in the olivine grains are common and parallel, the serpentinization and formation of lizardite veins also occur in parallel with these regular fractures and finally form the band texture of the olivine (28). With the removal of pressure and an increase in the volume of peridotite rocks, regular and multifaceted fractures are formed in olivine by the fluid flow of the fractures (29). They begin to grow, with more fluid penetrating the fractures and continuing the process of serpentinization; lizardite grows in the same way as before and moves toward the center of the olivine. This cycle continues until there is no olivine left or the fluid enters is over.

Next, the remaining olivines between the mesh, hourglass, polygonal, or band textures are re-affected by the serpentinization process, and destroyed, leaving no grains and they have been substituted by serpentine and magnetite. The development of lizardite in the central part can depend on factors such as the difference in fluid composition at this stage compared to the previous stage, the difference in temperature and pressure conditions during the reaction, or the difference in olivine composition in the center relative to the margin (30). The studied samples are similar to those of Oman ophiolite mantle peridotites and serpentinized ophiolites of Kerman province, which tolerate 60% serpentinization

and include mesh and pseudomorphic textures containing chrysotile and magnetite streaks (31). Fabric for relative preferential orientation has also been observed in these rocks. Schistosity is caused by the orientation of serpentine grains, which can result from simultaneous growth with their tectonics (32). At the boundary of the olivine fragments, due to stretching, empty spaces are created that are suitable for the growth of any serpentine mineral. In serpentinite, due to serpentine sheet minerals, when the stress is received, the sheets slide on top of each other and form regular processes. By forming a preferential orientation, both horizontal (slippery) and vertical (slightly elongated) stresses are better tolerated by the rock. The ribbon or strip growth of chrysotiles has also been observed in rocks in meso- and microscopic samples, usually accompanied by veins and masses of magnetite. This texture may be related to deformations that correspond with the replacement of rocks on the ground. When orthopyroxene crystals have become bastitization, or the remnants of intact olivine crystals act as porphyroclasts and serpentines with a striped texture are placed around the crystal, the ocular texture is formed.

The Gysian serpentinite mineralogy (chrysotile and magnetite) is similar to the Alpine serpentinites of Auckland (33). It shows that these rocks have not further subducted to the degree of antigorite formation and have formed at temperatures below 300° C (34). In the following stages, with tectonic action and thrust faults in the region and dehydrating and increasing the rock volume (35) and consequently decreasing the density (36), the ascent to the surface has occurred. This stage is accompanied by deformation and the occurrence of transverse fractures at the ultramafic boundary and may have destroyed some previous fabrics and intensified the sheeted appearance of the rocks, causing the chromite (Cr-spinels) to fragment. The formation of network textures and filling of veins with calcite has also occurred at this stage and near the surface. In contrast, mesh and bastite textures are formed in the first stages of serpentinitization.

Discussion

A close look at the microstructure of serpentinites

In the absence of obvious deformation, serpentinites in the form of isotropic rocks have a mesh texture at the matrix that hosts the bastite blades. Networks usually have specific cores and margins. Bastites and lattice nuclei often have similar mineralogy, a combination of serpentine minerals, including chrysotile, polygonal serpentine, proto serpentine, and lizardite blades. In the core of the networks, the serpentine has a random

orientation, while in the bastite, regular (nanometer-thick) lizardite blades may fill the space between the random serpentines. The lattice rim is more crystalline than anywhere else and consists of lizardite micrometer fragments with an axis perpendicular to the core/rim boundary (37). Thus, in networks, lizardite often grows in regular directions, both of which are detected by compensator blades in a polarizing microscope. The lizardite (001) plates are usually maintained from one network to another, creating a three-dimensional interlocking skeleton with two vertical CPO plates. In Gysian serpentinites, as in the same case (in southern Tuscany, Italy), the thickness of the blue and yellow margins is almost equal in all rocks, and the volume occupied by the nucleus (pink) is larger than the space created by the margins (Figure 3). These fine and precise mineralogical and microstructural differences in the location of minerals have a significant effect on the local strength of serpentinites and cause heterogeneous responses by the rock to stresses (38).

In some Gysian samples, deformable traces have been found in the bastites (Figure 4 a, b), which are folds and kinking in the bastite blades marked by the cleavage levels of pyroxenes. Brittle deformation was also sometimes observed, leading to cracks in the bastites and through which chrysotile veins of the strip or blade type passed (39) (Figure 4 c-g). The progression of the deformity led to more rounding of the bastites and bypassing the lizardite (001) plates around the bastites, which itself created an augen texture (Figure 4 h). Considering the predominant phase of chrysotile and referring to grade petrogenetic diagrams (40) to know the stability field of chrysotile mineral, it is known that the maximum temperature of this mineral is 300 to 400° C at low to medium pressures (less than 10 kbar) (34). Therefore, in the absence of antigorite in these rocks, the depth at which Gysian serpentinites were formed was more minor than 50 km.

An overview of the Mineral chemistry and Whole-rock geochemistry

To achieve the composition of the main minerals in the rocks, several samples were analyzed as EPMA (45). Based on this, the remaining olivines were ferrohorthonolithic composition, Cr-spinels had the chromite composition, clinopyroxenes were hedenbergite, and orthopyroxenes were left over from serpentinitization were ferrosilite (41). The geochemistry of the Gysian rocks is similar to the mantle serpentinites studied along the Neo-Tethys, for example, with the serpentinites of Massio Voltri in the Italian Alps or with the average subducted

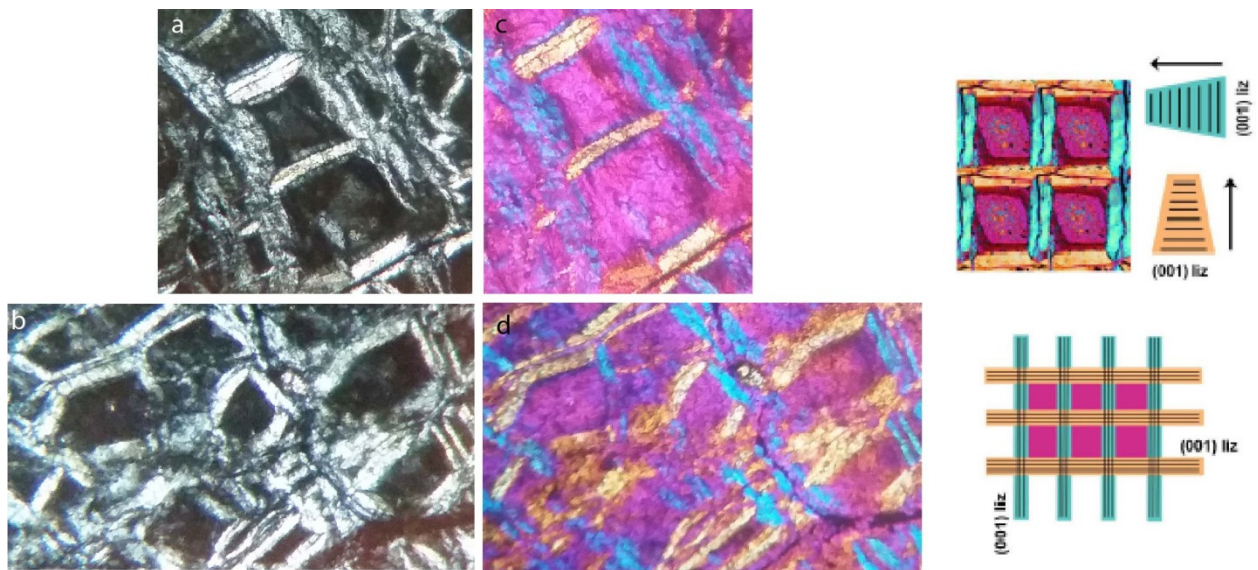


Figure 3. The Microstructures of mesh cells in the Gysian serpentinites. a and b are the cross-polarized photos and c and d taken after gypsum compensator use. The core of each cell, the pink area, is a less crystallized random matter which is surrounded by the lizardite [001] plates, in blue and yellow color.

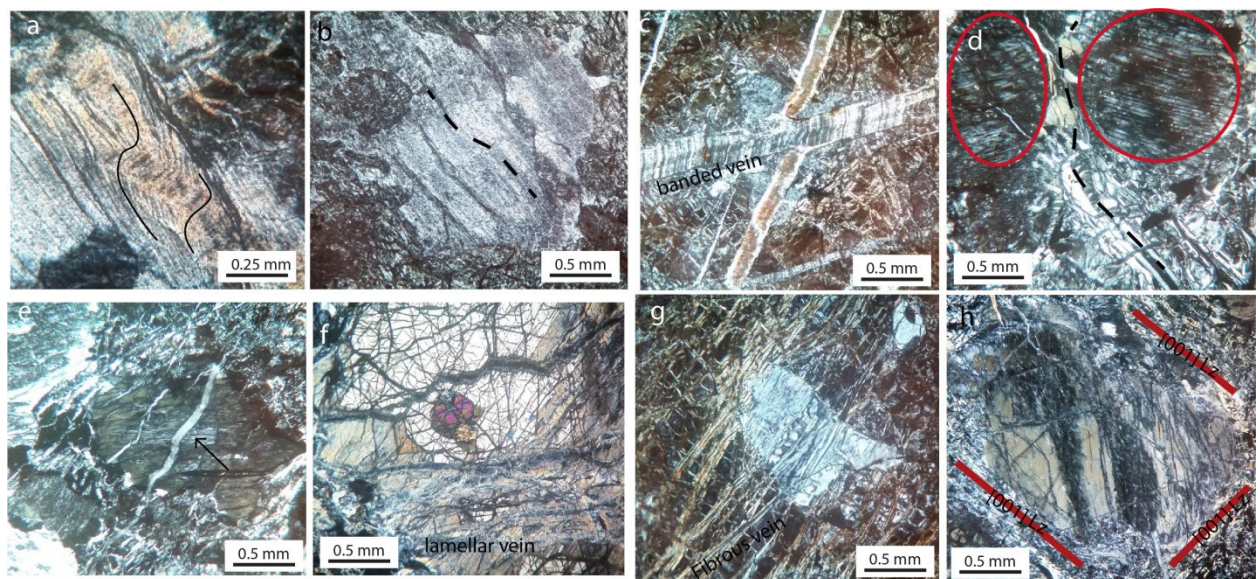


Figure 4. a, b Ductile deformation formed microfolds and kinks in bastites. c to g Brittle deformation including cracks, banded, lamellar and fibrous veins fragmented the bastites. h Progressive deformation formed rounding of bastites which are bypassed with [001] plates of lizardites and result in the augen texture. All of them are XPL.

serpentinites (42). These rocks are 95 to 100% serpentine and their LOI is about 12 to 13%. This number indicates their moderate to high serpentinization. In the triple chart based on LOI, the composition of Gysian serpentinites is precisely similar to the world average serpentinites and is very close to the global standard (UB-N) composition (43).

The content of intermediate metals such as Sc, V, Co,

Ni, Cr, and Cu in these rocks is significant, indicate high levels of olivine and orthopyroxene in the primary protolith and except for the negative anomaly of titanium in other elements similar to the primary mantle (44). Due to the low levels of titanium in these rocks, protoliths from dunite to harzburgite are evaluated. Referring to the geochemical characteristics of three types of serpentinites, including abyssal, mantle wedge, and

subducted, it is clear, especially in terms of the abundance of titanium (more than 30 to 150 ppm) and high Yb (0.1 to ppm), as well as significant enrichment of FME during refertilization, Gysian serpentinites are similar to subducted species (44).

CSD

The dynamic power of kinetic procedures in igneous rocks can be measured under-cooling or super-saturation of the association (45). The resulting crystal population is altered by mechanical factors such as sorting, coarsening, Ostwald ripening, or subsequent mixing (46). The primary functions that control growth textures are the nucleation rate, which is a function of time, and the growth rate, which depends on the time of growth and size. The common assumption is that the growth rate is independent of size. Of course, it is not always possible to ensure that the growth rate is not very dependent. For a crystal in such an environment:

$$n'_V(L) = n'_V(0)e^{-L/G\tau}$$

This is corresponding to the long dimension of all crystals with a linear CSD pattern of size zero to eternity. Items such as Ostwald-ripening in metamorphic rocks (10), mixing of two magmas in volcanic rocks (47), length of magma residence time (12), filter pressing, and crystal accumulations lead to variations and curve in the straight-line CSD pattern (46). The chromite crystals, because of their importance in crystallization history determination, different shapes and sizes in thin sections, characteristic crystals (Figure 5), and economic valuables in the Gysian serpentinites, are selected for CSD studies are selected.

We prepared a large sectional 2D image from the rocks using whole slide imaging (WSI) scanner. Then images are processed with Digimizer software to measure the width, length, area, and other physical data for chromites. To convert the 2D data to 3D, CSDCorrections (25) software is used, and CSD patterns are illustrated in Figure 6. CSD patterns for Gysian

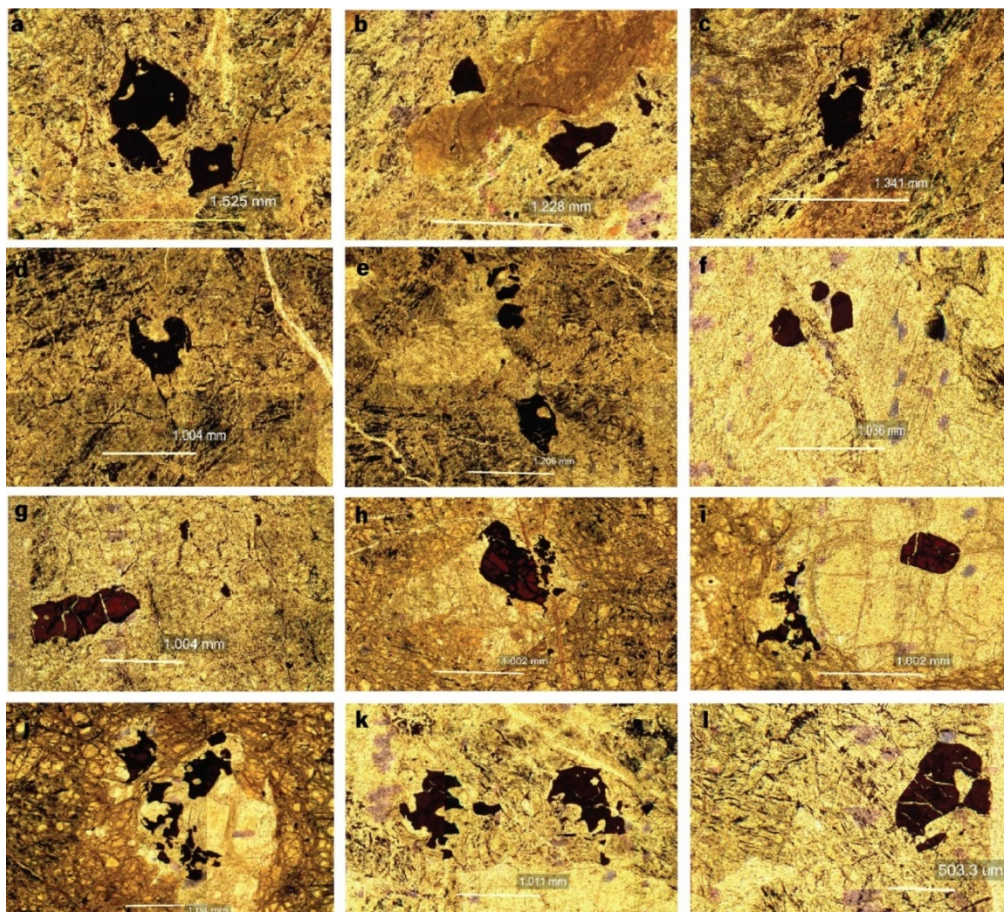


Figure 5. The chromatic spinels at the Gysian serpentinites. All of them gathered in PPL. The fragmentation due to the deformation and decompression in g, h, i, and l are clear.

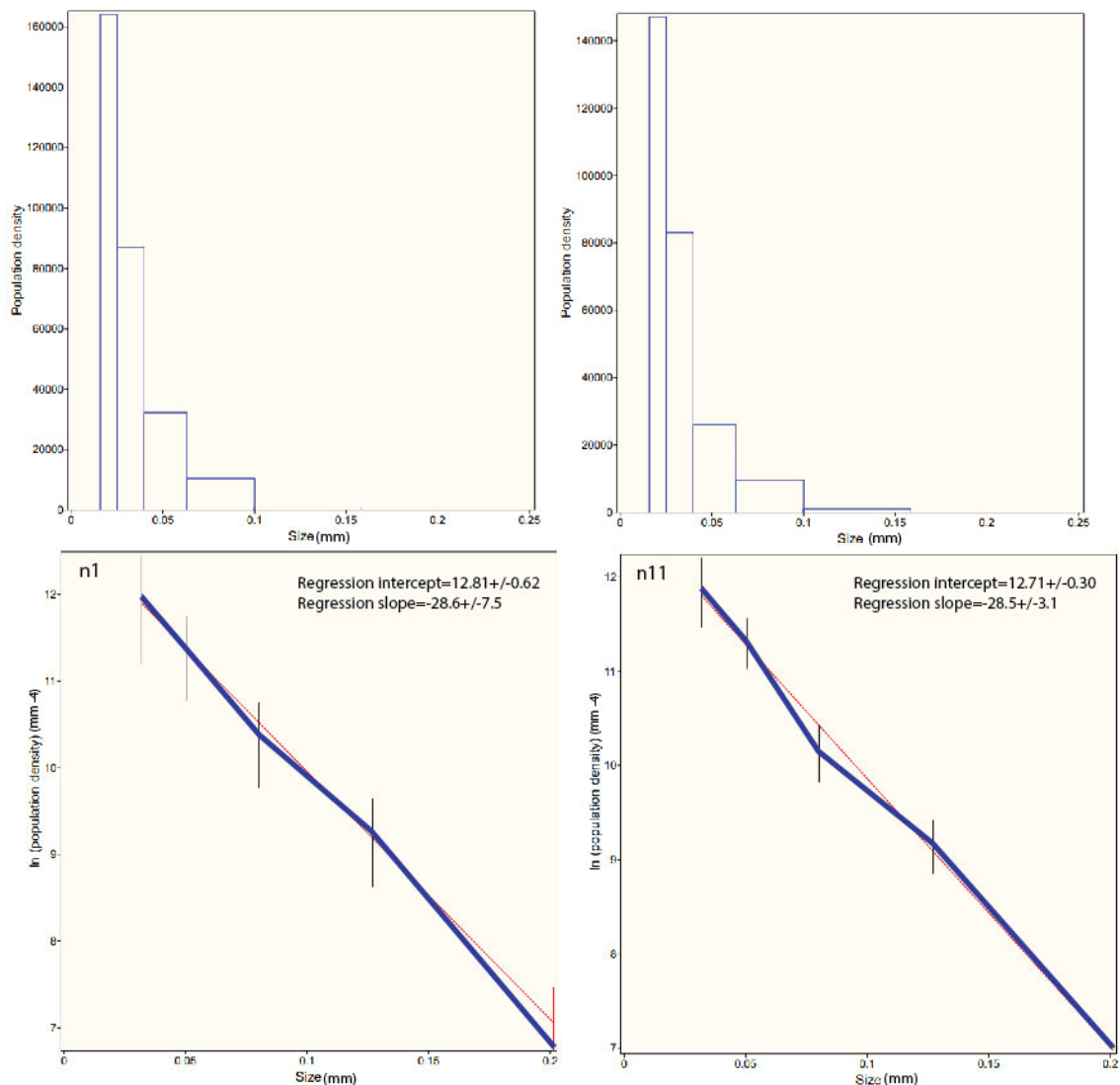


Figure 6. WSI photos of the thin sections, the crystal size histograms and CSD pattern of chromites in Gysian serpentinites. The intercept values (J/G) and slope of regression ($-1/Gt$) are written on the diagrams. There is typically one.

chromites are divided into three types: The first type is the linear pattern, which shows the steady-state crystallization with an intercept value of 12, which equals a nucleation rate/growth rate (J/G) of about 12. The regression slope is -28 which is related to the growth rate, and $Gt=1.28$ (Figure 6).

The second type has a non-linear concave down pattern which is the result of annealing or Ostwald ripening at a small size part with an intercept value of 13-15; therefore, $J/G=13-15$ and $Gt=1.33$ for them led to the slope of the pattern to be equal to -33 (Figure 6).

Coarsening connects the very small crystals to form a large crystal because of the grain boundary area reduction (GBAR) law. Another name for it is Ostwald ripening or

annealing (46). At the considerably deformed rocks, static recrystallization occurs on them, and if a fluid like water is available, it has measurable effects at lower temperatures. The Ostwald ripening caused the initial linear CSD pattern to change to a concave down form at the mean crystal size, and its shape only depends on the rate-adjusting growing. During this phenomenon, the small grains are dissolved and there is a decrease in the gain of large crystals (48). The small grains are unstable because of their high surface Gibbs free energy. If nucleation finishes and growth is possible, the CSD is affected by this ripening (48). It is a widespread occurrence in igneous crystallization. At these composite CSDs, we must interpret the patterns segment by

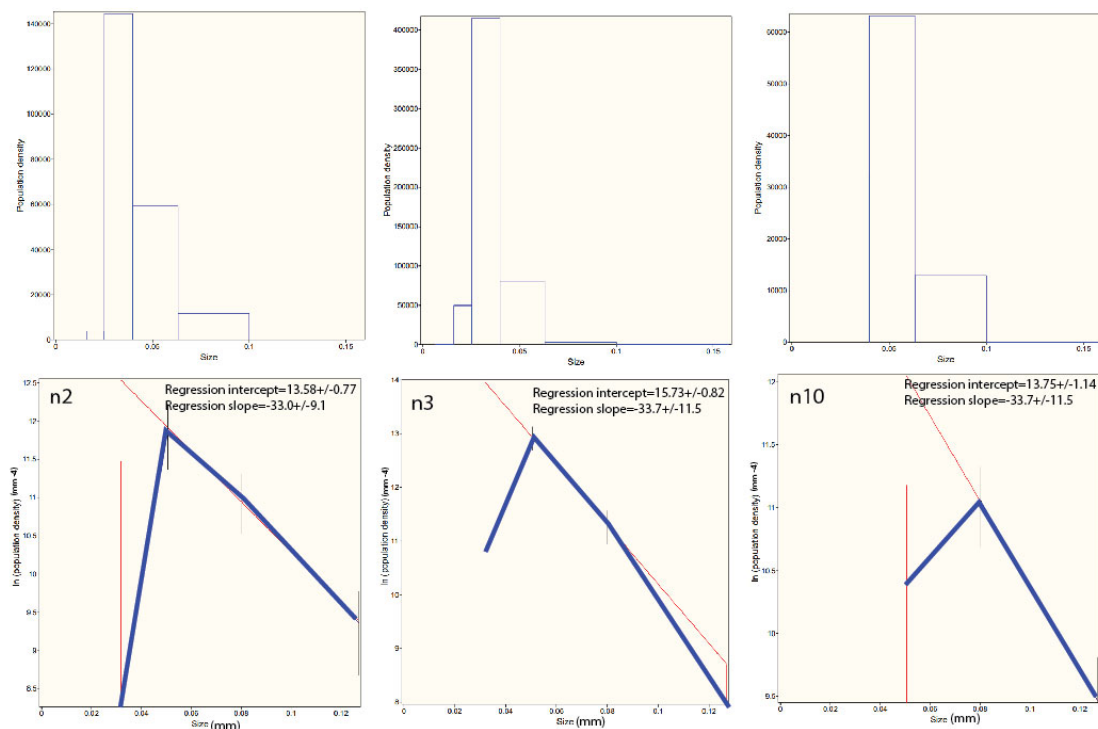


Figure 6. Continued. There is type two with annealing.

segment, and extract of nucleation and growth history is more complicated.

In the second type of CSD of chromites of serpentinites, we observe a single nucleation event followed by ripening during nucleation. Also, post-emplacement annealing may occur rapidly on them. As a result of the resorption of smaller grains, we show a curved pattern on the beginning part of the CSDs.

The third type is more complex and shows two population densities. It could be modeled by two crystal populations, small and large sizes which formed concave-up CSD patterns (Figure 6). The intercept value for small sizes is 12-18 demonstrating that the J/G is 12 to 18 for small crystals. The slope of the patterns for the small part is -40 to -60, indicating a range of Gt from 1.40 to 1.60. For large crystals, intercept values of 9-10 show the J/G to be 9-10 times for them and the slope of -7 to -10 shows that Gt is 1.7 to 1.10 for the large population. The J/G of small crystals is more than large ones, and thus, it is predicted that their growth is less. Considering the constant growth rate for crystals, from silicate materials, 10^{-9} cm/s or 10^{-10} cm/s, and using a slope of the patterns, it is determined that the growth of large chromites is six times longer than that of small crystals. The small crystals may be produced during arising of the residual peridotites or when the mafic minerals such as olivine or pyroxenes alteration exist. In the petrography

part, we show some coarse grains which are fragmented and cracked during arising (Figure 5). It is possible that these occurrences caused an increase in the rate of small grains, too.

Conclusion

One of the components of the Gysian Silvana ophiolite, south of Urmia near Iran's border with Turkey and Iraq, is serpentinites at the continuance of the Neo-Tethys suture zone. The significant phases are chrysotile, and magnetite and some rare cr-spinels (chromite), orthopyroxene, and clinopyroxene coexist among them. Almost all the peridotitic rocks are serpentinitized, and only remnants of mafic minerals remain. Several microstructures show stress and deformation tolerance in these rocks. One of them is the lizardite plates across the mass nucleus of less crystallized serpentine, which was discovered with the help of the compensator. Due to the lack of antigorite in these rocks, the subduction depth in this part of the Neo-Tethys was probably less than 50 km. This indicates the high gradient of the oceanic slab in the northern part of the Neo-Tethys in Iran and the reason for mélangé formation in ophiolite in this section of suture. In these rocks, the chromite size distribution was also investigated, and three types of patterns were separated including straight-line type, convex-up coarsening symptom, and a combination of two statistical

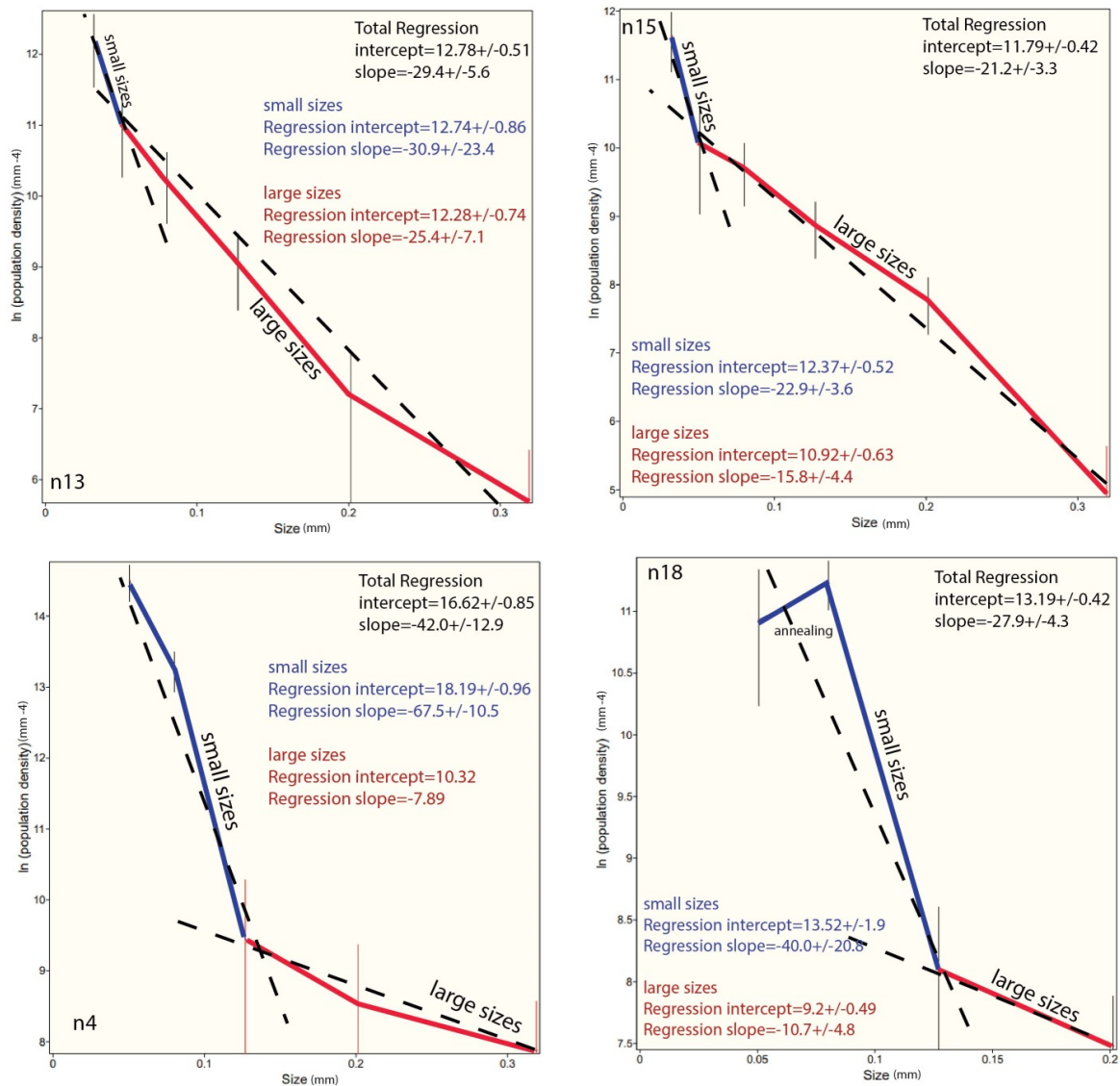


Figure 6. Continued for type three with two population densities.

populations. After the initial crystallization at steady-state (type one), annealing (Ostwald ripening), and co-integration of finer grains, they are constraining concave up in the fine grain part of the CSD pattern (type two). In some rocks, there is evidence of two categories of coarse and fine crystals with two intercept values and different pattern slopes. Such samples may have been caused by the fragmentation of coarse chromite grains confirming an increase in the number of fine grains or the creation of fine crystals due to deformation when rock arises, and decompression and alteration of mafic minerals like olivine take place. The result is that CSD patterns should be interpreted segment by segment and can never be given a general opinion for the whole pattern, especially

when it has a composite shape.

Acknowledgments

The author thanks the editors and reviewers of the Journal. The author received financial support from the Natural Science Foundation of Urmia University.

References

- Alexeiev DV, Kröner A, Hegner E, Rojas-Agramonte Y. Middle to Late Ordovician arc system in the Kyrgyz Middle Tianshan: From arc-continent collision to subsequent evolution of a Paleozoic continental margin. Gondwana

- Res. 2016;39:261-291.
2. Faure M, Lin W, Chu Y, Lepvrier C. Triassic tectonics of the southern margin of the South China Block. *Comptes Rendus Geoscience*. 2016;348(1):5-14.
 3. McCollom TM, Bach W. Thermodynamic constraints on hydrogen generation during serpentinization of ultramafic rocks: *Geochim Cosmochim Acta*. 2009;73(3):856-875.
 4. Frost BR, Evans KA, Swapp SM, Beard JS and Mothersole FE. The process of serpentinization in dunite from New Caledonia. *Lithos*. 2013;178:24-39.
 5. Hilairat N, Reynard B, Wang Y, Daniel I, Merkel S, Nishiyama N, Petitgirard S. High-pressure creep of serpentine, interseismic deformation, and initiation of subduction. *Science*. 2007;318(5858):1910-1913.
 6. Hattori KH and Guillot S. Volcanic fronts form as a consequence of serpentinite dehydration in the forearc mantle wedge. *Geology*. 2003;31(6):525-528.
 7. Tatsumi Y. The subduction factory: how it operates in the evolving Earth. *GSA Today*. 2005;15(7):4.
 8. Mével C. Serpentinization of abyssal peridotites at mid-ocean ridges. *Comptes Rendus Géoscience*. 2003;335:825-852.
 9. Bach W, Garrido CJ, Paulick H, Harvey J, Rosner M. Seawater-peridotite interactions: first insights from ODP Leg 209, MAR 15°N. *Geochemistry, Geophysics, Geosystems*. 2004;5(9):22.
 10. Modjarrad M. Geochemistry and crystal shape, size and spatial distribution in arc-related gabbro, Urmia, NW Iran. *Geochimica Acta*. 2022a; DOI: 10.1007/s11631-022-00557-8.
 11. Moazzen M, Modjarrad M. Contact metamorphism and crystal size distribution studies in the Shivar aureole, NW Iran. *Geol J*. 2005;40:499-517.
 12. Modjarrad M. Crystal size distribution of amphiboles from Bezow dacites, Urmia, Iran. *Neues Jahrbuch Fur Geologie Und Palaontologie Abhandlungen*. 2015;276:101-110.
 13. Modjarrad M, Sheykhbaglou S. Crystal size distribution of amphibole and plagioclase from Zanbil adakitic dacites, Urmia-Iran: Evidence for magma mixing and textural coarsening. *Acta Geodynamic Geomaterials*. 2016;181:89-101.
 14. Cashman KV, Ferry JM. Crystal size distribution (CSD) in rocks and the kinetics and dynamics of crystallization III. Metamorphic crystallization. *Contribut Mineral Petrol*. 1988;99:410.
 15. Hajmolla Ali A, Shahrabi M. Geological map of Silvana, N. 4964. Geological Survey of Iran. 2006; Tehran.
 16. Sheikholeslami MR. Deformations of Palaeozoic and Mesozoic rocks in southern Sirjan, Sanandaj-Sirjan Zone, Iran. *J Asian Earth Sci*. 2015;106:130-149.
 17. Alavi M. Regional stratigraphy of the Zagros fold-thrust belt of Iran and its proforeland evolution. *Am J Sci*. 2004;304(1):1-20.
 18. Allen MB, Kheirkhah M, Emami MH, Jones SJ. Right-lateral shear across Iran and kinematic change in the Arabia-Eurasia collision zone. *Geophysic J Int*. 2011;184(2):555-574.
 19. Aziz H, Asahara Y. Juvenile granite in the Sanandaj-Sirjan Zone, NW Iran: Late Jurassic-Early Cretaceous arc-continent collision. *Int Geol Rev*. 2013;55:1523-1540.
 20. Golonka J. Plate tectonic evolution of the southern margin of Eurasia in the Mesozoic and Cenozoic. *Tectonophysics*. 2004;381(1-4):235-273.
 21. Golonka J, Oszczytko N, Ślącza A. Late Carboniferous-Neogene geodynamic evolution and paleogeography of the circum-Carpathian region and adjacent areas. *Ann Societat Geologorum Poloniae*. 2000;70(2):107-136.
 22. Robertson AHF, Clift PD, Degnan PJ, Jones G. Palaeogeographic and palaeotectonic evolution of the Eastern Mediterranean Neotethys. *Palaeogeography Palaeoclimatol Palaeoecol*. 1991;87(1-4):289-343.
 23. Eren Rizeli M, Wang KL, Bingol AF, Beyarslan M. Mineral chemistry and petrology of mantle peridotites from the Guleman ophiolite (SE Anatolia, Turkey): evidence of a fore arc setting. 13th International Conference on Gondwana to Asia, At: Trivandrum, India. 2016;22.
 24. Shafaii Moghadam H, Li QL, Stern RJ, Chiaradia M, Karsli O, Rahimzadeh B. The Paleogene Ophiolite Conundrum of the Iran-Iraq Border Region. *J Geol Soc*. 2020.
 25. Alizadeh A. Dating of the southern Urmia colored mélange. 30th symposium of Earth Sciences of Iran 2012; Tehran.
 26. Higgins MD. Measurement of crystal size distributions. *Am Mineral*. 2000;85:1105-16.
 27. Page BM, De Vito LA, Coleman RG. Tectonic emplacement of serpentinite southeast of San Jose, California. *Int Geol Rev*. 1999;41:494-505.
 28. Azer MK, Khalil AE S. Petrological and mineralogical studies of Pan-African serpentinites at Bir Al-Edeid area, Central Eastern Desert, Egypt. *J Afr Earth Sci*. 2005;43(5):525-536.
 29. Francis GH. The serpentinite mass in Glen Urquhart, Invernesshire, Scotland. *Am J Sci*. 1956;254:201-226
 30. Hopkinson L, Beard JS and Boulter CA. The hydrothermal plumbing of a serpentinite-hosted detachment: Evidence from the West Iberia non-volcanic rifted continental margin. *Marine Geol*. 2004;204:301-315.
 31. Boudier F, Baronnet A, Mainprice D. Serpentine mineral replacements of natural olivine and their seismic implications: Oceanic lizardite versus subduction-related antigorite. *J Petrol*. 2009;51(1-2):495-512.
 32. Mohammadi N, Ahmadipour H, Peighambari S. Investigation of deformational behavior of serpentinites in Baft ophiolitic malange (Kerman) and its effects on the seismic potential of the region. *Iran J Geol*. 2013;6(24):3-17.
 33. Reinen LA. Seismic and aseismic slip indicators in serpentinite gouge. *Geology*. 2000;28(2):135-138.
 34. O'Brien J, Rodgers KA. Alpine-type serpentinites from the Auckland Province—III. Petrography, mineralogy, petrochemistry, and petrogenesis. *J Royal Soc New Zealand*. 1974;4(2):141-159.
 35. Evans BW. The serpentinite multisystem revised: chrysotile is metastable. *Int Geol Rev*. 2004;46:479-506.
 36. Iyer K, Austrheim H, John T, Jamtveit B. Serpentinization of the oceanic lithosphere and some geochemical consequences: constraints from the Leka Ophiolite Complex, Norway. *Chem Geol*. 2008;249:66-90.
 37. Christensen NI. Serpentinites, peridotites, and seismology. *Int Geol Rev*. 2004;46(9):795-816.
 38. Viti C, Mellini M. Mesh textures and bastites in the Elba retrograde serpentinites. *Eur J Mineral*. 1998;10:1341-1359.

39. Viti C, Collettini C, Tessei T, Tarling MS, Smith S. Deformation Processes, Textural Evolution and Weakening in Retrograde Serpentinites. *Minerals*. 2018;8:241.
40. Roumejon S, Cannat M, Pierre Agrinier P, Godard M, Andreani M. Serpentinization and Fluid Pathways in Tectonically Exhumed Peridotites from the Southwest Indian Ridge (62–65-E). *J Petrol*. 2015;56(4):703-734.
41. Bromiley GD, Pawley AR. The stability of antigorite in the systems MgO–SiO₂–H₂O (MSH) and MgO–Al₂O₃–SiO₂–H₂O (MASH): the effects of Al³⁺ substitution on high pressure stability. *Am Mineral*. 2003;88:99–108.
42. Rezaie MDA, Modjarrad M (2018). The Ultramafic rocks of Silvana ophiolite. 25th symposium of crystallography and mineralogy of Iran. 2018; Yazd, Iran.
43. Deschamps F, Godard M, Guillot S, Hattori K. Geochemistry of subduction zone serpentinites: A review. *Lithos*. 2013;178:96-127.
44. Abdollah K, and Modjarrad M. Serpentinites of Ziveh Gysian south of Urmia, 3th international Congress of Earth Sciences of Iran. 2018; Tehran.
45. Modjarrad M. Petrology of the Maku - Poldasht young lavas: Attitude to the olivine and bubbles sizedistribution. *Applied Geochemistry (AAG)*, in press 2022b; (in Persian).
46. Cashman KV. Crystal Size Distribution (CSD) Analysis of Volcanic Samples: Advances and Challenges. *Front Earth Sci*. 2020;8.
47. Higgins MD. Quantitative textural measurements in igneous and metamorphic petrology. Cambridge University Press. 2006; New York, 277p.
48. Modjarrad M. Crystal size distribution studies on the leucite, pyroxene and olivine at the eastern Urmia Lake volcanic rocks- magma mixing possibility and residence time at the chamber. *Iran J Crystallography Mineral*. 2019;27:55-68 (in Persian).
49. Marsh BD. On the interpretation of crystal size distributions in magmatic systems. *J Petrol*. 1998;39:553–600.